# CHARACTERIZATION AND COMPUTATIONAL MODELING OF THE FRACTURING BEHAVIOR IN DISCONTINUOUS FIBER COMPOSITE STRUCTURES

Seunghyun Ko[1], Kenrick Chan[1], Reed Hawkins[2], Rohith Jayaram[2], Christopher Lynch[1], Reda El Mamoune[3], Minh Nguyen[1], Nicolay Pekhotin[1], Natania Stokes[1], Daniel N. Wu[4], Mark E. Tuttle[2], Jinkyu Yang[1], Marco Salviato[1]

[1]Department of Aeronautics and Astronautics, University of Washington
[2]Department of Mechanical Engineering, University of Washington
[3]Department of Materials Science and Engineering, University of Washington
[4]Department of Civil and Environmental Engineering, University of Washington
Guggenheim Hall
Seattle, WA 98185

## ABSTRACT

We investigate experimentally and numerically the size effect of discontinuous fiber composites (DFC) for two different unidirectional prepreg chip sizes (50×8 and 75×12 mm). We tested geometrically similar five different sizes of single-edge notched specimens with a constant thickness. We observed that fracture may happen away from the notch depending on the specimen sizes and chip sizes. To analyze such transitional notch sensitivity in the DFC, we use Bazant's size effect law. Experimental results are well fitted with the law, clearly showing the transition behavior of the DFC from being notch insensitive to sensitive. The transition of fracturing behavior implies that the design criteria of the DFC is shifting from strength-based to energy-based approaches. To obtain the fracture energy, $G_f$, we developed a finite element model based on the stochastic laminate analogy. The resulting $G_f$ for the DFC with the 75×12 mm chips is 22.2% higher than 50×8 mm chips. In conclusion, we show both the chip sizes and the structure size play an important role in fracturing behavior of the DFC.

## 1. INTRODUCTION

A discontinuous fiber composite (DFC) has an outstanding advantage in the manufacturing of complex structures within a very short period of time compared to the continuous fiber composite [1]. In a variety of industries including aerospace, automobile, and marine engineering, the DFC provides a new opportunity to design complex shapes using carbon fiber composite materials. However, there are still numerous unanswered questions about the DFC in terms of the relationship between the chip sizes and material properties, especially when the notch is present. Previous studies [2,3] have reported notch insensitivity in the DFC when cracking is involved. If this is valid for all DFC structures, it is a major problem for designing them because the failure location is unpredictable. Also, there are only limited amounts of information regarding the fracture property



*SAMPE Conference Proceedings. Long Beach, CA, May 21-24, 2018. Society for the Advancement of Material and Process Engineering – North America.*

of the DFC. Therefore, the current industry needs a design guideline for the DFC structures with the presence of notches.

In this paper, we investigate experimental and numerical study in fracturing behavior of the DFC using the size effect testing. We used two different chip sizes: 50×8 mm and 75×12 mm. We conducted single edge notch tension tests with five different geometrically scaled specimens. From the experimental results, we found that the notch sensitivity depends not only on the chip sizes but also on the structure sizes. Furthermore, using the size effect law [4,5] and the finite element model based on the stochastic laminate analogy [6,7,8], we found the intra-laminar fracture energy for the larger chip size is higher than the smaller chip size. Also, we calculated the length of the effective fracture process zone which provides a transition point from ductile to brittle behavior with increasing structure size. When the structure length was comparable with the effective fracture process zone (FPZ), it exhibited notch insensitive behavior. However, when the structure was large enough, the crack always initiated from the pre-existing notch. From our calculation, the larger chip size has a three times longer FPZ length compared to that of the smaller chip size. The following sections will explain the details of the size effect testing and the methods to calculate the fracture energy and the length of the effective FPZ.

## 2. MATERIAL MANUFACTURING

There are many commercially available DFCs today, including the Hexcel's HexMC. However, there are certain limitations to use the commercial products for the research purposes. First, the chip sizes are set to certain dimensions. Second, it is hard to control the thickness with the given prepreg form of the DFC. Therefore, we decided to develop a fully controllable, in-house manufacturing process. This allowed us to test the DFC with different chip sizes of our choosing. We validated the quality of the in-house manufacturing process by comparing the tensile modulus of the manufactured DFC with the calculated modulus of quasi-isotropic layup specimens. Throughout the study, we used Toray T700G-12K, 150 gsm with 35% resin content for the DFC manufacturing.

### 2.1 In-house manufacturing process

There were three main challenges in manufacturing the DFC. We needed to (1) control the chip sizes, (2) randomly but also evenly distribute the chips, and (3) manufacture a large amount of chips, in order of thousands of chips per panel. For example, a plate size of 400 x 400 $mm^2$ with 3 mm thickness requires 8600 chips with a size of 50×8 mm. We were able to address all three challenges using the CNC fabric cutter and the silicone coated parchment paper. We started with the cutting of two comb-shaped long strips from the unidirectional prepreg roll. Each strip had the width equal to the desired chip width. Then, the combs were separated from each other. After the separation, we made a tab at the end of the strips using the masking tape to ensure the strips are separated (Fig. 1a). To protect the surface of the prepreg, we used the silicone coated parchment paper. We removed the protective backing and covered the surface with another sheet of the parchment paper (Fig. 1b). The silicone coating eased the removal of the paper from the resin after the cutting was done. We cross-cut the comb-shaped strips covered with the parchment papers on both sides using the CNC fabric cutter (Fig. 1c, manufactured by Autometrix Advantage). Since all the cutting was done using the CNC machine, it guaranteed an accurate size of individual chips. We removed a side of the parchment paper from the prepreg and manually shake them into the container which was covered with a plastic bag (Fig. 1e). We randomly distributed the chips by

varying the shaking direction and by rotating the container after a certain period. We repeated the process until the DFC batch reached the desired weight. We debulked the DFC batch by applying 100 kPa of vacuum pressure for two hours. Debulking was the crucial step because void creation was a large source of defeats during the manufacturing process. The final batch is shown in Fig. 1f. The final batch was transported to the aluminum molds to be cured using the hot press. The ramping cycle was the following: 4.5 ºC/min up to 270ºC, hold 270 ºC for two hours, and 9 ºC/min cooling to the room temperature. Throughout the cycle, we used 0.61 MPa for the pressure. The final batch was trimmed 15 mm from the outside edge to discard any uncured regions. We used MK diamond wet tile saw instead of the water-jet to minimize the delamination around the specimens.

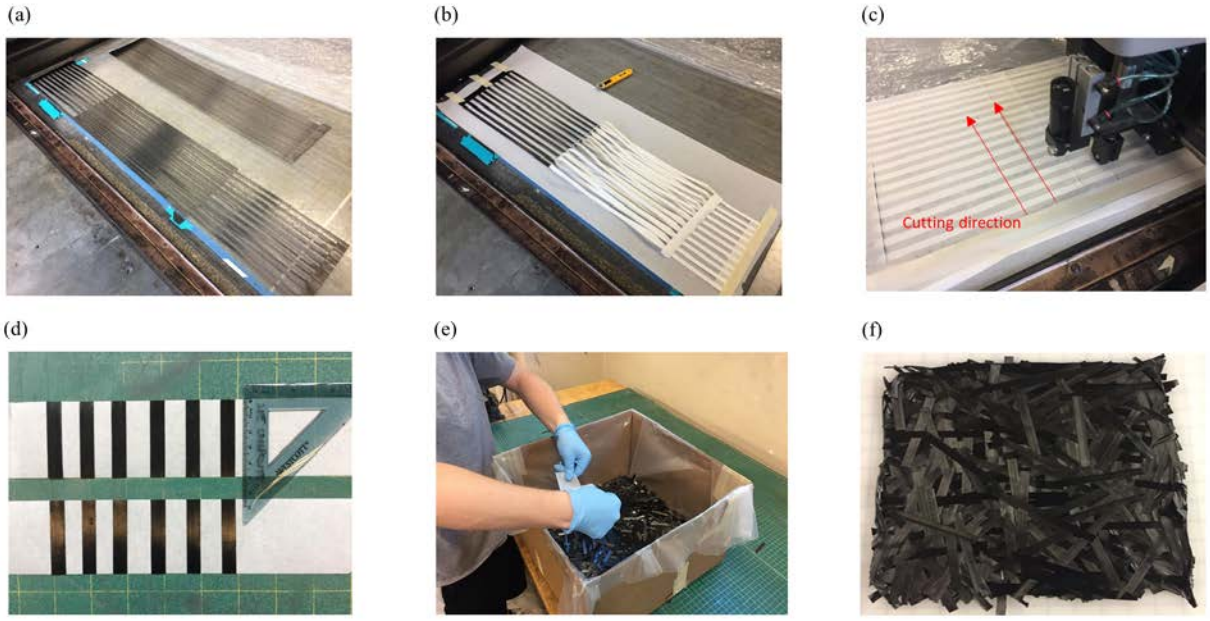


**Figure 1.** Digital images of the manufacturing process of the DFC.

## 2.2 Material property validation

We conducted uniaxial tensile tests on the smooth specimens following the ASTM D3039 to check the quality of the in-house manufactured DFCs. A Shore Western servo-hydraulic machine with a 155 kN capacity was used. The strain rate was set to be 0.2 %/min to make sure that each test does not last longer than 10 min. A total of 11 specimens with 50×8 mm chip size was tested. The specimen dimensions and the averaged results are shown in Table 1.

**Table 1.** Results of tensile tests on smooth specimens.

| | **Width (mm)** | **Gauge length (mm)** | **Total length (mm)** | **Ave. thickness (mm)** | **Ave. modulus (MPa)** |
|---|---|---|---|---|---|
| **DFC** | 26 | 120 | 250 | 3.56 | 45.04 ± 4.87 |

According to the reference [2], the Hexcel's HexMC provides the tensile modulus approximately 80% of the quasi-isotropic layup. We can estimate the quasi-isotropic tensile modulus of T700G using the published data [9]. The calculated quasi-isotropic tensile modulus is 54.87 MPa. The tensile modulus of in-house manufactured DFC reaches 82.1% of the calculated quasi-isotropic layup, which validates the quality of the manufacturing process.

# 3. TEST DESCRIPTION

## 3.1 Specimen geometry

The geometry of the single edge notch tension (SENT) specimens for the size effect tests were adapted from Bazant et al. [4] and Salviato et al. [5]. We tested five different sizes of the specimens, geometrically scaled in two-dimensions (width and gauge length) with the constant thickness. We took the 20-mm specimen as a reference (see Fig. 2) and scaled up to 6 which was the maximum specimen size from the current manufacturing setup. All the specimens had an equal ratio between gauge length L, width D, and the initial crack length $a_0$ which was 11.125:5:1. The tab length remained the same to ensure enough gripping area for the fixtures. The details of the geometry are listed in Table 2. To create a sharp notch, we used Zona 35-050 ultra-thin razor saws with 0.2 mm thickness. For the large specimens (size-1 and -2), we used Zona 35-300 medium razor saws with 0.38 mm thickness because the depth of the ultra-thin saw was limited. Increasing the thickness of the notch for the large specimens did not have a noticeable impact on the results because the size of the specimen was already large enough compared to the notch thickness.

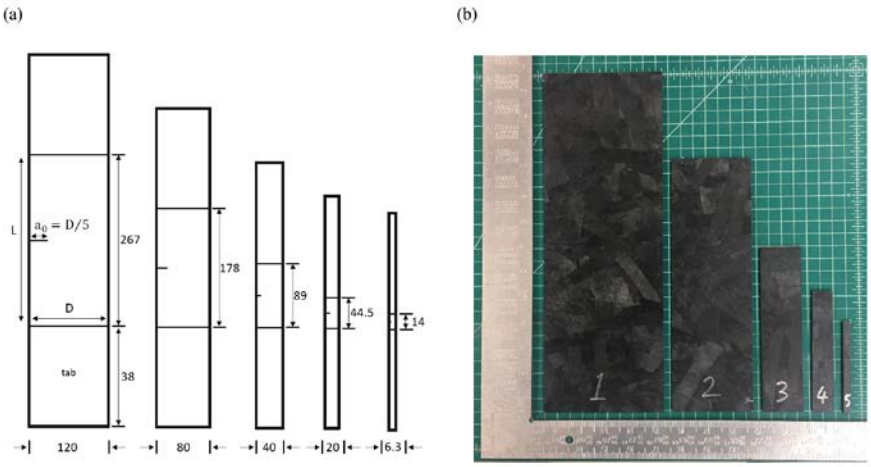


**Figure 2.** Geometry of single edge notch tension specimens (left) and the DFC specimens (right). Units: mm.

**Table 2.** Geometrical details of SENT specimens.

| Size | Width, $D$ (mm) | Gauge length, $L$ (mm) | Total length, $L+L_{tab}$ (mm) | Crack length, $a_0$ (mm) | Thickness, $t$ (mm) |
|---|---|---|---|---|---|
| **5** | 6.3 | 14 | 90 | 1.3 | 3.3 |
| **4** | 20 | 44.5 | 120.5 | 4 | 3.3 |
| **3** | 40 | 89 | 165 | 8 | 3.3 |

| | | | | | |
|---|---|---|---|---|---|
| **2** | 80 | 178 | 254 | 16 | 3.3 |
| **1** | 120 | 267 | 343 | 24 | 3.3 |

### 3.2 Experimental details

We used a servo-hydraulic Instron machine with a 200 kN capacity and a constant crosshead rate. We used the displacement rate of 0.15 mm/min for the size-4 specimens and linearly scaled the displacement rate for the different specimen sizes. The fixtures for the size-1 and -2 were different from the rest because of the limited fixture width. Instead, two parallel plates with the one side of gripping teeth are used. Two screws with a diameter of 19.05 mm connected the specimen and the plates directly (see Fig. 4c). Six additional screws tightened the surrounding tab area with the fixtures. No slippage was found throughout the tests.

## 4. EXPERIMENTAL RESULTS

We analyzed the load and displacement data for the different sizes of the specimens. In Fig. 3, typical load-displacement plots for 75×12 mm chip sizes are reported. We can easily recognize the decrease of nonlinearity as the structure size increases. The largest specimen is linear up to the peak loads indicating the brittle behavior. The smallest specimen has the strongest nonlinearity before the peak load indicating reduced brittle behavior.

The fracture surfaces of different sizes showed very distinct characteristics. The most noticeable feature was the notch sensitivity depending on the structure size. Previous studies [2,3] reported that the DFC shows strong notch insensitive behaviors. We were able to observe the notch insensitive behaviors in most of the size-4 and -5 specimens (Fig. 4a, b). However, as the structure size increased, a strong notch sensitivity was observed too (Fig. 4b, c). Also, the crack path became more perpendicular to the loading direction as the specimen size increased. These observations indicate the stress concentration around the notch becomes the dominant fracture component as the structure size increases. For the small structure sizes, the entire gauge area can be a potential fracture initiation zone. The inherent flaws in the structure such as resin pockets and voids become the strong fracture components along with the existing notch. Therefore, we were able to observe the notch insensitivity from the small specimen sizes. For the future research, we plan to study the effects of the defects using the micro CT scan to visualize such effects.

The SENT results are summarized in Table 3 and 4. We defined the nominal strength as the average stress at the failure within the un-notched cross sectional area. The test results clearly show the decreasing trend of the nominal stress with the increasing structure size in both chip-size cases. If we try to explain this trend in terms of the strength-based failure criteria such as Tsai-Wu or Tsai-Hill, it is not intuitive to do so. Furthermore, linear elastic fracture mechanics (LEFM) is not sufficient enough to explain the decreasing strength because according to the LEFM, the strength should decrease linearly proportional to $D^{-1/2}$. In our case, however, we find the nominal strengths remain stagnant in small width cases. Therefore, we use Bazant's size effect law [4] to analyze the test results of the DFC.

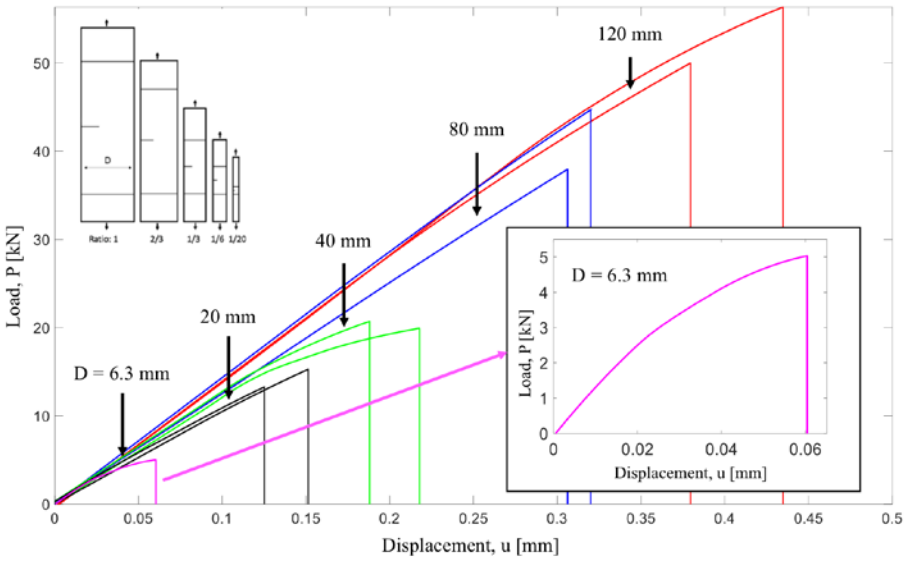


**Figure 3.** Load-displacement plots for geometrically scaled specimens with 75×12 mm chip sizes. Notice that the nonlinearity decreases as the structure size increases.

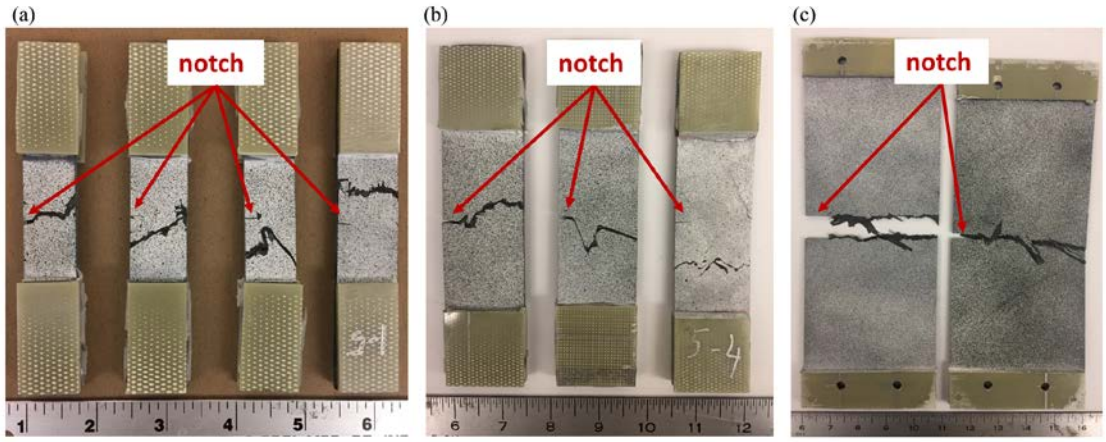


**Figure 4.** Fracture surfaces of geometrically-scaled SENT specimens with 50×8 mm chip sizes. (a) Size-4, *D* = 20 mm, (b) Size-3, *D* = 40 mm, and (c) Size-1, *D* =120 mm.

**Table 3.** Results of SENT for the 50×8 mm chip size.

| Size | Gauge length, $L$ (mm) | Width, $D$ (mm) | Max. load, $P_{max}$ (N) | Nominal strength, $\sigma_N$ (MPa) |
|---|---|---|---|---|
| **5** | 14 | 6.3 | 5221.3 ± 384.9 | 243.0 ± 20.1 |
| **4** | 44.5 | 20 | 15264.7 ± 4652.5 | 248.4 ± 54.3 |
| **3** | 89 | 40 | 25371.1 ± 2079.2 | 194.8 ± 15.5 |
| **2** | 178 | 80 | 39707.8 ± 5073.4 | 153.8 ± 27.6 |
| **1** | 267 | 120 | 56125.1 ± 4499.4 | 139.1 ± 15.6 |

**Table 4.** Results of SENT for the 75×12 mm chip size.

| Size | Gauge length, $L$ (mm) | Width, $D$ (mm) | Max. load, $P_{max}$ (N) | Nominal strength, $\sigma_N$ (MPa) |
|---|---|---|---|---|
| **5** | 14 | 6.3 | 5216.4 ± 536.0 | 230.2 ± 29.1 |
| **4** | 44.5 | 20 | 10327.5 ± 6221.8 | 212.4 ± 26.6 |
| **3** | 89 | 40 | 22433.5 ± 4600.5 | 177.5 ± 29.3 |
| **2** | 178 | 80 | 45305.8 ± 6358.0 | 167.7 ± 27.1 |
| **1** | 267 | 120 | 60168.7 ± 7928.2 | 143.1 ± 16.5 |

# 5. DISCUSSION

## 5.1 Analysis of size effect tests using Bazant's size effect law

We analyzed the foregoing experimental results using Bazant's type II size effect law (SEL) [4]. The SEL relates the nominal strength $\sigma_N$ in terms of the characteristic size of the structure. In this case, we choose the width of the specimen D as the characteristic size. We adopt an equivalent linear elastic fracture mechanics approach to relate $\sigma_N$ to $D$ using two material properties (fracture energy, $G_f$ and effective fracture process zone length, $c_f$) and the structure shape properties (dimensionless energy release rate $g(\alpha)$ and $g'(\alpha)$).

Starting with the LEFM, we relate the energy release rate in terms of the relative crack length:

$$G(\alpha) = \frac{\sigma_N^2 D}{E^*} g(\alpha) \qquad [1]$$

We define the parameters used in the Eq. (1) as the following: $\alpha = a/D$ = normalized effective crack length where $a$ is the crack length, $\sigma_N = P/(Db)$ where $P$ is load applied, $b$ is the thickness,

$E^* = E$ for plane stress and $E/(1-\upsilon^2)$ for plane strain, and $g(\alpha)$ = dimensionless energy release rate. The failure of the structure can be written using an effective crack length $a = a_0 + c_f$ where $a_0$ = initial crack length and $c_f$ = effective FPZ length which is assumed to be a material property. Substituting this into Eq. (1), we can define the fracture energy, $G_f$, in terms of the effective crack length:

$$G\left(\alpha_0 + c_f/D\right) = \frac{\sigma_N^2 D}{E^*} g\left(\alpha_0 + c_f/D\right) = G_f \qquad [2]$$

$G_f$ in this particular study is the mode I intra-laminar fracture energy of the material. By approximating the $g(\alpha)$ with its Taylor expansion at $\alpha_0$ and remain only up to the linear term, we have the following expression of $G_f$:

$$G_f = \frac{\sigma_N^2 D}{E^*}\left[g(\alpha_0) + \frac{c_f}{D} g'(\alpha_0)\right] \qquad [3]$$

Here, $g'(\alpha_0) = \mathrm{d}g(\alpha_0)/\mathrm{d}\alpha$. Reorganize the Eq. (3), we have an expression of the nominal strength in terms of material properties, and the structure size $D$.

$$\sigma_N = \sqrt{\frac{E^* G_f}{D g(\alpha_0) + c_f g'(\alpha_0)}} \qquad [4]$$

Equation (4) can be further simplified to match with the size effect law [4,5].

$$\sigma_N = \frac{\sigma_0}{\sqrt{1 + D/D_0}}, \qquad \text{where } \sigma_0 = \sqrt{\frac{E^* G_f}{c_f g'(\alpha_0)}} \text{ and } D_0 = c_f \frac{g'(\alpha_0)}{g(\alpha_0)} \qquad [5]$$

Here, $\sigma_0$ and $D_0$ become constants depending on the FPZ size and the specimen geometry for homogeneous material [5]. However, the DFC is non-homogeneous material due to the irregular chip deposition. Therefore, as we will discuss further, a series of $g(\alpha_0)$ and $g'(\alpha_0)$ are computed using the finite element model to obtain the average values of $g(\alpha_0)$ and $g'(\alpha_0)$. The averaged values are relatively close to each other within 10% of coefficients of variation, meaning that the SEL still holds well for this material.

Equation (5) shows the dependence of the nominal strength in terms of the structure size $D$. However, unlike classical LEFM where the nominal strength is linearly proportional to $D^{-1/2}$, Eq. (5) includes the characteristic length $D_0$. This characteristic length distinguishes between the classical LEFM and the SEL because it can describe the change in the behavior of the structure from ductile to brittle as the structure size increases.

### *5.1.1 Linear regression analysis of SEL*

We can obtain the SEL parameters using the linear regression analysis. In order to do so, it is convenient to define the following terms:

$$X = D, Y = \sigma_N^{-2} \quad [6]$$

$$\sigma_0 = C^{-1/2}, D_0 = \frac{C}{A} = \frac{1}{A(\sigma_0)^2} \quad [7]$$

Using Eq. (6) and (7), the SEL can be expressed in a simple linear form:

$$Y = C + AX \quad [8]$$

By plotting the experimental results following the Eq. (6), we obtained the constants for Eq. (7) (see Fig. 5). For the 50×8 mm chip size, $\sigma_0$ = 0.269 GPa and $D_0$ = 40.45 mm. For the 75×12 mm chip size, $\sigma_0$ = 0.225 GPa and $D_0$ = 76.01 mm. We plotted the experimental results of SENT tests using Eq. (5) and (7) on Fig. 6 where the normalized nominal strength $\sigma_N/\sigma_0$ was plotted as a function of the normalized characteristic size $D/D_0$ in a double logarithmic scale. A horizontal asymptote represents the strength criterion where there is no size effect or length dependency. An asymptote of slope -1/2 represents the LEFM. The intersection point where $D = D_0$ represents the transitional size.

From Fig. 6, we observe three important results. (1) The failure of the DFC containing the traction-free notch expresses a strong size effect. (2) The size effect shows a gradual decrease in nominal strength with increasing size of the structure. It is a transition from the strength-based criterion to the energy-based criterion. (3) The chip size has a strong influence on the fracturing behavior of the DFC. The larger chip size shows more ductile response whereas the smaller chip size exhibits a more brittle response. Also, using the SEL, we can explain why some of the previous studies [2,3] observed notch insensitive fracturing behavior of the DFC. If the structure size is small enough that the FPZ size becomes comparable with the structure size $D$ (or the structure size is far smaller than $D_0$), the material behaves in a notch insensitive manner. Therefore, the relative size of the structure and the FPZ must be taken into account when we design with the failure of the DFC.

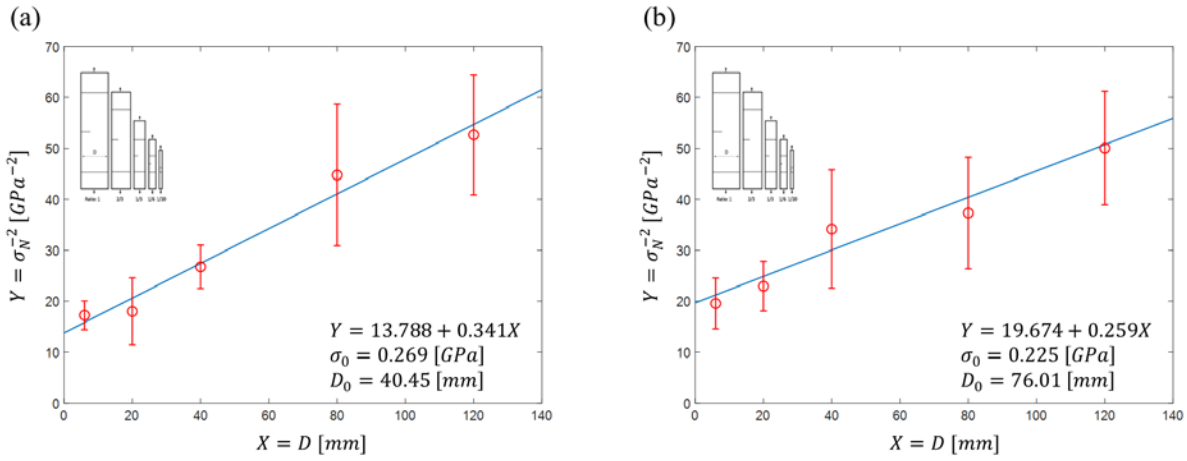


**Figure 5.** Linear regression analysis of the experimental results to find the size effect parameters. (a) 50×8 mm chip, (b) 75×12 mm chip.

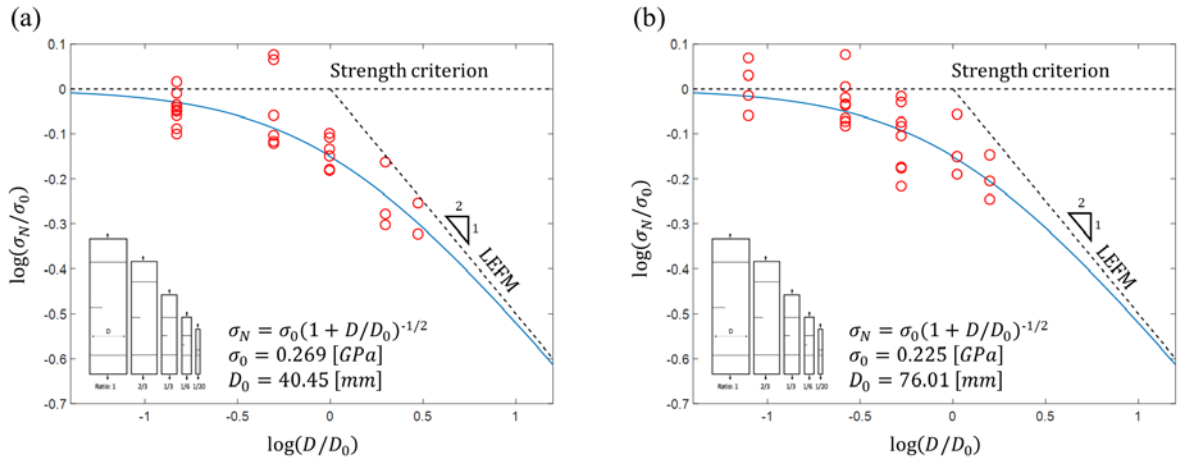


**Figure 6.** The size effect of the DFC with (a) 50×8 mm chip, (b) 75×12 mm chip.

# 6. DEVELOPMENT OF A FINITE ELEMENT MODEL

In order to calculate the dimensionless energy release rate $g(\alpha)$ and its derivative $g'(\alpha)$, we developed a 2D finite element model using the stochastic laminate analogy. The stochastic laminate analogy generates series of randomly oriented plies and combines them as a homogeneous laminate using the classical laminate theory [6]. Feraboli et al. [7] and Harban et al. [8] applied the analogy to the DFC structures to simulate the material properties such as the in-plane ultimate strength and the in-plane modulus. They proposed the idea to simulate random morphology of the DFC by dividing the structure into multiple representative volume elements (RVE) or partitions with randomly chosen laminate orientations. Selezneva et al. [10] stepped further by explicitly generating the chips with random orientations and locations, and stored the chip information to each corresponding RVE. This method generated a smooth transition of the local stiffness between adjacent RVEs which in result provided a more accurate imitation of the DFC's morphology. We adopted Selezneva's model and further improved it by proposing the resin layer inclusion method and the chip saturation method to eliminate unrealistic ply thickness adjustments and enforcing even chip distribution.

## 6.1 Random chip generation and distribution details

We first generated the random morphology using Matlab [11]. The code randomly chose a center location of the chip and the orientation. We chose the normal distribution for statistical variations. But the distribution can easily be adapted by any statistical variations if necessary. The chip information was stored in the partitions which were later exported to Abaqus [12]. Figure 7 presents a basic morphology of the chip on top of the partitions. The chip generation stopped after the average number of chips within a certain area reached the target chip average. The target chip average was equal to the total thickness divided by the chip thickness, in this case, equaled to 24. Due to the random characteristics of the chip generation, each partition had a different number of chips with a unique set of orientations. Since each partition's total thickness was set to be uniform, the individual ply thickness was adjusted accordingly. When the number of chips reached beyond the target chip average, individual ply thickness decreased linearly to match the thickness of the target chip average (3.3 mm). However, when the number of chips was lower than the target

average chip, we did not linearly increase the thickness of the plies. Instead, we inserted resin layers in between the plies to match the target average thickness. The resin layer had isotropic properties equal to the matrix, therefore, the total stiffness of the structure was not significantly affected by its inclusion. This resin inclusion method avoided the unrealistic increasing of ply thickness which can significantly affect the modulus. Figure 7b summarizes the layer adjustment.

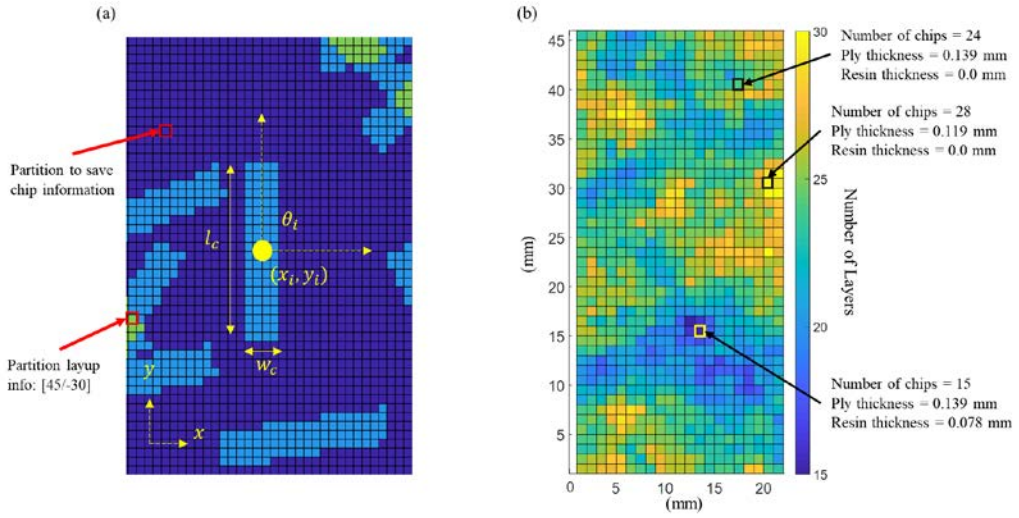


**Figure 7.** (a) Individual chips was randomly generated and stored into partitions. (b) Individual ply thickness and resin layers were adjusted according to the target chip average (= 24 plies with 3.3 mm thickness).

Another unique chip morphology generation technique that we developed is the chip saturation method. As we mentioned before, there are stochastic variations in the number of chips between partitions. In certain regions, the number of average chips is extremely low or extremely high, causing unrealistic representative morphology of the DFC. These phenomena are caused by uncontrolled depositions of the chips in a given space. In order to prevent such cases, we created multiple stopping points (called saturation limit points) on the average number of chips through the thickness during the random generation scheme. The chip generation scheme can only pass the limit points when the certain number of iterations was passed without any further deposition of chips (Fig. 8a). The limit points forced the chip generation scheme to find the locations of the low number of chips in the geometry for additional chip deposition. It prevented unrealistic shortages in the number of chips in certain partitions (see Fig. 8). Also, to limit the unrealistic concentrations of chips, we limited the deposition of chips in certain partitions if they had reached a maximum amount of chips. The maximum number of chips were chosen based on the number of chips that we counted using the microscope. This causes the skewed distribution in Fig. 8b. The summary of the morphology generation algorithm is summarized in Fig. 9.

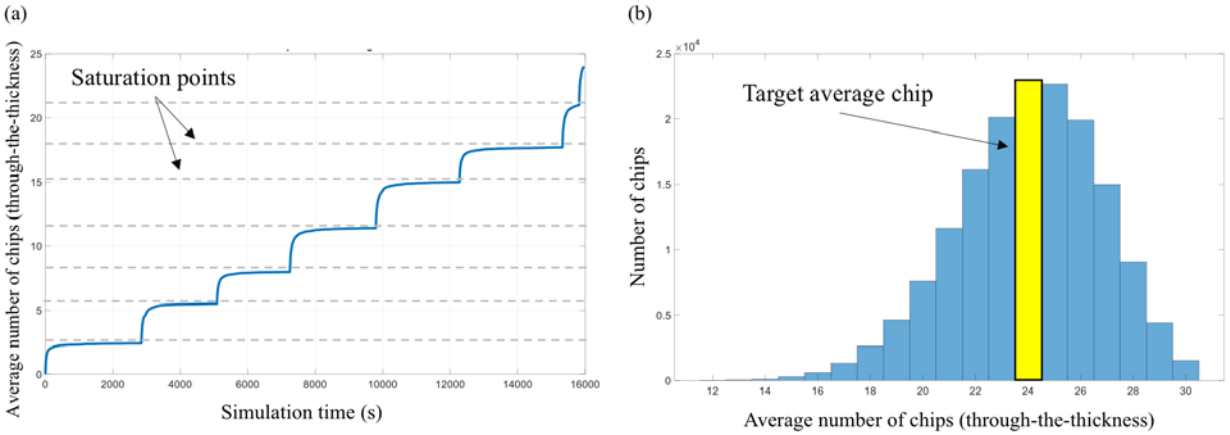


**Figure 8.** (a) Saturation limit points allow even distribution of chips through given space. (b) Results of the saturation limit points eliminate unrealistic concentrations or absences of chips.

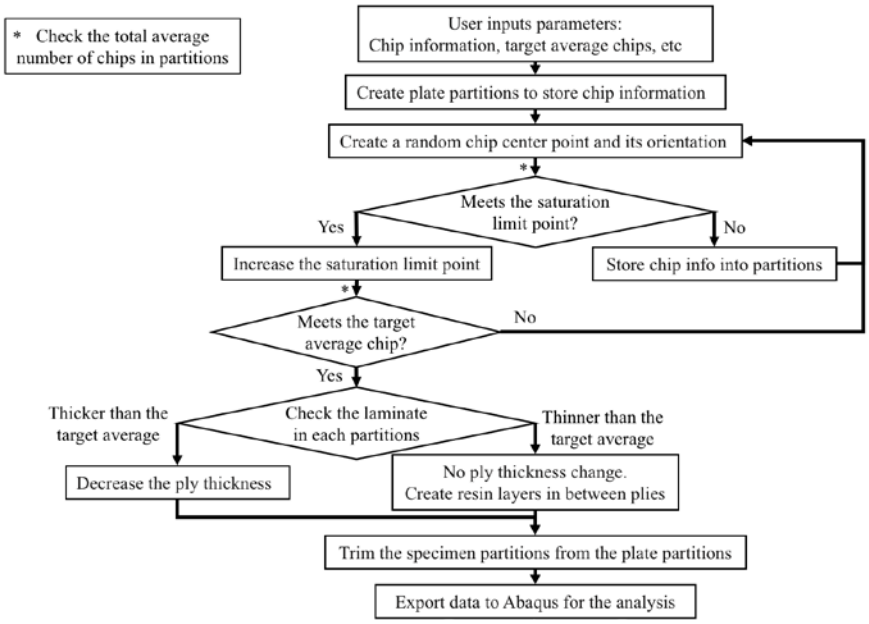


**Figure 9.** DFC morphology generation algorithm flow chart

## 6.2 Calculation of $g(\alpha_0)$, $g'(\alpha_0)$, and $G_f$

After the completion of the chip generation scheme, partitions information were transferred to Abaqus/Standard. Abaqus imported the individual chip orientations and thickness, built sets of laminates and assigned them to the plate geometry. We used eight-node shell elements (S8R) for the analysis. We fixed all the directions at the end of geometry except vertical displacement to apply the displacement. The J-integral approach to find the energy release rate was not applicable in this case because of inhomogeneous material characteristics. Therefore, the following expression was used to calculate the energy release rate [13]:

$$G(u,a) = -\frac{1}{b}\left[\frac{\partial \Pi(u,a)}{\partial a}\right]_u \quad [9]$$

In Eq. (9), $u$ is an equilibrium displacement, $b$ is thickness, $a$ is a crack length, and $\Pi$ is the potential energy. We obtained the series of potential energy or internal energy of the entire structure from Abaqus by increasing the crack length but keeping the constantly applied displacement. Using the central difference scheme, we obtained $G(\alpha)$. Then, we calculated $g(\alpha)$ using Eq. (9):

$$g(\alpha) = \frac{G(\alpha)E^*}{\sigma_N^2 D} \quad [9]$$

Figure 10 shows an example of $g(\alpha)$ for a single specimen. We use a linear regression analysis to obtain $g'(\alpha)$. In this particular example, $g(\alpha_0 = 0.2)$ = 0.816 and $g'(\alpha_0 = 0.2)$ = 4.795.

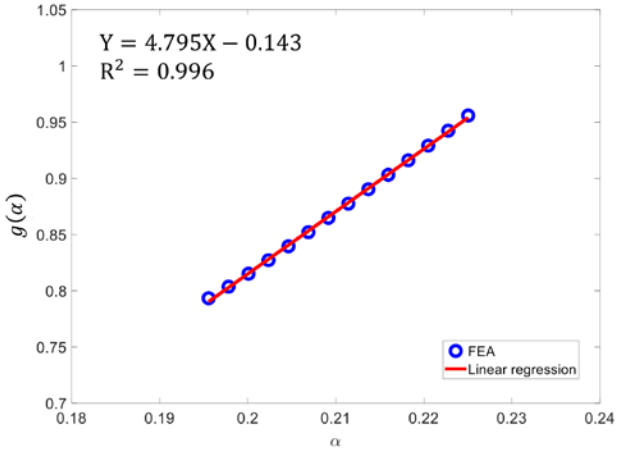


**Figure 10.** The results of the dimensionless energy release rate $g(\alpha)$ from FE model. $g'(\alpha)$ is calculated using a linear regression analysis.

We calculated the fracture energy $G_f$ and the effective FPZ length $c_f$ for DFC specimens with 50×8 mm chip sizes and 75×12 mm chip sizes using Eq. (5) and obtained $g(\alpha)$ and $g'(\alpha)$ (see Table 5). The fracture energy $G_f$ and the effective FPZ length $c_f$ show significant differences between the two chip sizes. $G_f$ increases by 25.1% and $c_f$ shows a 168.4% increase. A significant increase in the length of the FPZ explains the ductile behavior of the DFC specimens with larger chip sizes.

**Table 5.** Fracture properties of the DFC with different chip sizes using the SEL.

| **Chip Size (mm)** | $g(\alpha_0)$ | $g'(\alpha_0)$ | **Fracture energy, Gf (N/mm)** | **Effective FPZ length, $c_f$ (mm)** |
|---|---|---|---|---|
| **50×8** | 0.89 ± 0.09 | 5.36 ± 0.63 | 52.66 ± 5.60 | 5.31 ± 0.63 |
| **75×12** | 0.85 ± 0.04 | 4.62 ± 0.62 | 65.84 ± 2.68 | 14.25 ± 1.77 |

# 7. CONCLUSIONS

In this paper, we investigate and discuss the intra-laminar size effect of the DFC with two different chip sizes (50×8 and 75×12 mm). We make the following conclusions based on the size effect experiments and the finite element model using the stochastic laminate analogy.

1. From the experimental results of the geometrically-scaled single edge notch specimens, we observe a strong size effect in the DFC. By increasing the size of the test specimen, the fracturing behavior of the DFC shows a smooth transition from ductile to brittle.
2. The intensity of quasi-brittleness in the DFC depends on the chip size. We observe that having a larger chip size (75×12 mm) makes the structure behaves in a more ductile manner. The DFC with a smaller chip size (50×8 mm) fractures in a more brittle manner.
3. We obtain the initial fracture energy $G_f$ and the effective fracture process zone (FPZ) length $c_f$ for the DFC using the size effect tests and the finite element analysis. The finite element model provides the dimensionless energy release rate. The $G_f$ of the DFC with 50×8 mm chip size is 52.66 ± 5.60 N/mm with $c_f$ equal to 5.31 ± 0.63 mm. The $G_f$ of the DFC with 75×12 mm chip size is 65.84 ± 2.68 N/mm with $c_f$ equal to 14.25 ± 1.77 mm. We can conclude that the chip size strongly influences both $G_f$ and $c_f$.
4. We recommend using the larger chips when the structure has pre-existing notches because the larger chips have a higher $G_f$ and fracture in more ductile way.


## ACKNOWLEGEMENTS

We acknowledge the financial support by the FAA-funded Center of Excellence for Advanced Materials in Transport Aircraft Structures (AMTAS) and The Boeing Company. We thank the project monitors for their support and guidance: Ahmet Oztekin, Cindy Ashforth, and Larry Ilcewicz from the FAA, and William Avery from the Boeing Company. We also thank technical support provided by Bruno Boursier from the Hexcel Corporation, Bill Kuykendall and Michelle Hickner in Mechanical Engineering at the University of Washington.

# 8. REFERENCES


1. Boursier B., “New possibilities with HexMC, a high performance moulding compound,” *22nd SAMPE European conference*, March 2001.
2. Boursier, B., Lopez, A., “Failure initiation and effect of defects in structural discontinuous fiber composites,” *SAMPE*. Seattle, Washington, 2010.
3. Feraboli, P., Peitso, E., Cleveland, T., Stickler, P., Halpin, J.C., “Notched behavior of prepreg-based discontinuous carbon fiber/epoxy systems,” *Comp. Part A.* 40 (2009) 289-299.
4. Bazant, Z.P., Daniel, I.M., Li, Z., “Size effect and fracture characteristics of composite laminates,” *J. Eng. Mater. Technol.* 118 (3) (1996) 317-324.
5. Salviato, M., Kirane, K., Ashari S.E., Bazant, Z.P., Cusatis, G., “Experimental and numerical investigation of intra-laminar energy dissipation and size effect in two-dimensional textile composites”, *Comp. Sci. and Technol*. 135 (2016) 67-75.
6. Halpin, J.C., Pagano, N.J., “The laminate approximation for randomly oriented short fiber composites,” *J. of Comp. Mat.*, vol.3 (1969), 70.
7. Feraboli, P., Cleveland, T., Stickler, P., Halpin, J., “Stochastic laminate analogy for simulating the variability in modulus of discontinuous composite materials,” *Comp. Part A.* 41 (2010) 557-570.
8. Harban K., Tuttle M., “Reducing certification costs of discontinuous fiber composite structures via stochastic modeling,” *U.S. Department of Transportation Federal Aviation Administration*, May 2017.
9. Toray Composite Materials America, Inc. T700G preliminary data sheet.
10. Selezneva, M., Roy, S., Meldrum, S., Lessard, L., Yousefpour, A., “Modelling of mechanical properties of randomly oriented strand thermoplastic composites,” *J. of Comp. Mat.*, 51 (2017), 831-845.
11. The MathWorks, Inc., “Matlab 2016b,” The MathWorks, Inc., Natick, 2016.
12. ABAQUS, v., Abaqus User Manual, Version 6.13-1, Hibbit, Karlson and Sorenson, Pawtucket, RI. (2013).
13. Bazant, Z.P., Planas, J., “Fracture and size effect in concrete and other quasibrittle materials,” CRC press, 1998.